



# Atomically Local Electric Field Induced Interface Water Reorientation for Alkaline Hydrogen Evolution Reaction

*Chao Cai<sup>†</sup>, Kang Liu<sup>†</sup>, Long Zhang<sup>†</sup>, Fangbiao Li, Yao Tan, Pengcheng Li, Yanqiu Wang, Maoyu Wang, Zhenxing Feng, Debora Motta Meira, Wenqiang Qu, Andrei Stefancu, Wenzhang Li, Hongmei Li, Junwei Fu,<sup>\*</sup> Hui Wang,<sup>\*</sup> Dengsong Zhang,<sup>\*</sup> Emiliano Cortés,<sup>\*</sup> and Min Liu<sup>\*</sup>*

**Abstract:** The slow water dissociation process in alkaline electrolyte severely limits the kinetics of HER. The orientation of H<sub>2</sub>O is well known to affect the dissociation process, but H<sub>2</sub>O orientation is hard to control because of its random distribution. Herein, an atomically asymmetric local electric field was designed by IrRu dizygotic single-atom sites (IrRu DSACs) to tune the H<sub>2</sub>O adsorption configuration and orientation, thus optimizing its dissociation process. The electric field intensity of IrRu DSACs is over  $4.00 \times 10^{10}$  N/C. The ab initio molecular dynamics simulations combined with in situ Raman spectroscopy analysis on the adsorption behavior of H<sub>2</sub>O show that the M–H bond length (M = active site) is shortened at the interface due to the strong local electric field gradient and the optimized water orientation promotes the dissociation process of interfacial water. This work provides a new way to explore the role of single atomic sites in alkaline hydrogen evolution reaction.

## Introduction

Alkaline water electrolysis is a promising way for large-scale hydrogen production.<sup>[1]</sup> In alkaline electrolyte, water dissociation as the source of hydrogen is generally regarded as the rate-determining step for hydrogen evolution reaction (HER).<sup>[2]</sup> Generally, the orientation of H<sub>2</sub>O, including the adsorption configuration (O-down or H-down) and the H–O–H bond angle of H<sub>2</sub>O, at the interface between catalyst and electrolyte can directly affect the dissociation process.<sup>[3]</sup> Therefore, regulating the orientation of interface H<sub>2</sub>O to facilitate the H<sub>2</sub>O dissociation could be a promising way to enhance the HER activity.

H<sub>2</sub>O molecule is a typical polar molecule, which can be easily polarized under the action of electric field.<sup>[4]</sup> The polarized H<sub>2</sub>O molecules will undergo orientation rearrangement, from a randomly H<sub>2</sub>O adsorbed phase to a uniform configuration. In particular, the H-down configuration can shorten the distance between the active site (M) and H and enhance the M–H binding energy,<sup>[5]</sup> which is beneficial to the dissociation process of interfacial H<sub>2</sub>O molecules.<sup>[6,7]</sup> Through regulating the charge transfer between active sites and the surrounding atoms, it is possible to tune the local electric field around the active site to

[\*] C. Cai,<sup>\*</sup> K. Liu,<sup>\*</sup> L. Zhang,<sup>\*</sup> F. Li, Y. Tan, P. Li, H. Li, J. Fu, H. Wang, M. Liu

Hunan Joint International Research Center for Carbon Dioxide Resource Utilization, School of Physics and Electronics, Central South University  
Changsha 410083, Hunan (P. R. China)  
E-mail: fujunwei@csu.edu.cn  
huiwang@csu.edu.cn  
minliu@csu.edu.cn

Y. Wang, W. Li  
School of Chemistry and Chemical Engineering, Central South University  
Changsha 410083, Hunan (P. R. China)

M. Wang, Z. Feng  
School of Chemical, Biological, and Environmental Engineering, Oregon State University  
Corvallis, OR 97331 (USA)

M. Wang, D. Motta Meira  
X-ray Science Division, Advanced Photon Source, Argonne National Laboratory  
Argonne, IL 60439 (USA)

W. Qu, D. Zhang

International Joint Laboratory of Catalytic Chemistry, Department of Chemistry, Research Center of Nanoscience and Technology, College of Sciences, Shanghai University  
Shanghai 200444 (P. R. China)  
E-mail: dszhang@shu.edu.cn

A. Stefancu, H. Li, E. Cortés  
Nanoinstitut München, Fakultät für Physik, Ludwig-Maximilians-Universität München  
80539 München (Germany)  
E-mail: Emiliano.Cortes@lmu.de

[†] These authors contributed equally to this work.

© 2023 The Authors. Angewandte Chemie International Edition published by Wiley-VCH GmbH. This is an open access article under the terms of the Creative Commons Attribution License, which permits use, distribution and reproduction in any medium, provided the original work is properly cited.

optimize the  $\text{H}_2\text{O}$  orientation and enhance its dissociation process.<sup>[8]</sup>

In this work, we originally designed Ir/Ru dizygotic single-atom sites on CoP catalysts (IrRu DSACs) to generate an atomically asymmetric local electric field for tuning the  $\text{H}_2\text{O}$  adsorption configuration and orientation, and thus promoting the alkaline HER. The double Cs-corrected scanning transmission electron microscopy (STEM) directly characterized the atomic-scale charge and local electric field distribution around the active sites. The IrRu DSACs possess a high charge density variation of  $4.00 \text{ e} \text{\AA}^{-2}$ , corresponding to an electric field intensity of  $\approx 4.00 \times 10^{10} \text{ N/C}$ , much larger than  $2.24$  and  $2.12 \text{ e} \text{\AA}^{-2}$  of Ru and Ir SACs, respectively. The ab initio molecular dynamics (AIMD) simulations further revealed the impact that the atomically localized electric field has on the re-orientation of water at the interface, including the configuration evolution of adsorbed  $\text{H}_2\text{O}$ , and the M–H distance change. The in situ Raman characterization confirmed the asymmetric H-down adsorbed  $\text{H}_2\text{O}$  configuration with an increased H–O–H bond angle, which are positively correlated to the  $\text{H}_2\text{O}$  dissociation ability, indicating an excellent alkaline HER activity. As a result, the IrRu DSACs show an ultralow overpotential of  $10 \text{ mV}$  for achieving  $10 \text{ mA cm}^{-2}$  current density in a single cell, and a high stability over  $300 \text{ h}$  at  $1 \text{ A cm}^{-2}$  in a membrane electrode assembly (MEA). This work provides an unorthodox/original way to explore the role of local electric field on water dissociation for better HER.

## Results and Discussion

The interfacial  $\text{H}_2\text{O}$  reorientation induced by the asymmetrical atomical electric field is shown schematically in Figure 1. For pure CoP catalysts without strong local electric fields, the interfacial  $\text{H}_2\text{O}$  shows a random arrangement and the distance between Co and H ( $d_1$ ) is relatively large (Figure 1a). The Ir/Ru dizygotic single-atom sites on CoP catalysts (IrRu DSACs) lead to local charge transfer among Ru, Ir and CoP, resulting in a strong atomic electric field

around the Ir and Ru sites. Under the action of electric field, the interfacial  $\text{H}_2\text{O}$  molecules rearrange around the Ir/Ru DSACs, in an orderly phase. The distance between M site and H ( $d_2$ ) is apparently shorter than the corresponding  $d_1$  in the case of pure CoP.

The possible structure models of CoP and IrRu DSACs were constructed (Figure S1), in which the adjacent Ru and Ir sites constitute DSACs in the CoP matrix. The charge density analysis shows that the IrRu DSACs cause an intensive charge redistribution (Figure 2a), which leads to a strong and asymmetric atomic electric field. In order to study the effect of the local electric field on the orientation of interfacial  $\text{H}_2\text{O}$  molecules, the ab initio molecular dynamics (AIMD) simulations were performed. The local electric field around the IrRu DSAC affects the configuration of  $\text{H}_2\text{O}$  molecules and the distributions of H and O at the interface (Figure 2b). The average distance between H and surface of IrRu DSACs is significantly reduced from  $2.5 \text{ \AA}$  to  $1.6 \text{ \AA}$  (Figure 2c), while the distance between O and surface is not changed significantly in these two cases. These results reflect the orientation polarization of  $\text{H}_2\text{O}$  molecules on IrRu DSACs surface.

We further employ density functional theory (DFT) calculation to investigate the energy barrier for  $\text{H}_2\text{O}$  dissociation on the CoP and IrRu DSACs (Figure 2d and Table S1). The results show that the energy barrier of  $\text{H}_2\text{O}$  dissociation on the IrRu DSACs is  $0.68 \text{ eV}$  which is much lower than that on CoP ( $0.91 \text{ eV}$ ). Moreover, the IrRu DSACs enables an optimal hydrogen adsorption free energy ( $\Delta G_H$ ) of  $0.04 \text{ eV}$  which is much lower than that of CoP ( $0.36 \text{ eV}$ ) and very close to the ideal value ( $0 \text{ eV}$ , Figure S2 and S3). The above findings demonstrate that the interfacial  $\text{H}_2\text{O}$  reorientation induced by local electric field at the active site can optimize the  $\text{H}_2\text{O}$  dissociation process and H adsorption, therefore, improving the HER performance.

Encouraged by the theoretical prediction, we designed and prepared the IrRu DSACs by a simple impregnation-reduction method. The scanning electron microscopy (SEM) image shows a nanosheet structure of IrRu DSACs (Figure S4). The nanosheet substrate provides abundant anchoring sites for metal single-atom sites. Transmission electron

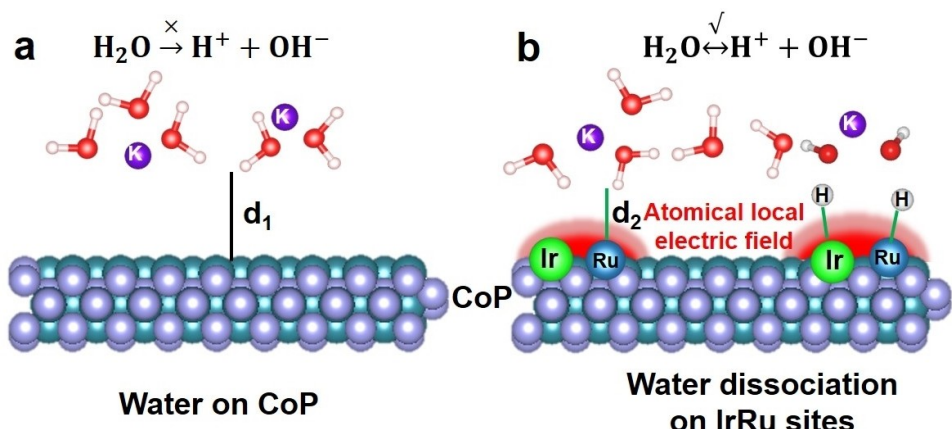


**Figure 1.** Schematic of interface  $\text{H}_2\text{O}$  reorientation induced by atomical electric field.  $\text{H}_2\text{O}$  adsorbed on a) CoP and b) IrRu DSACs.

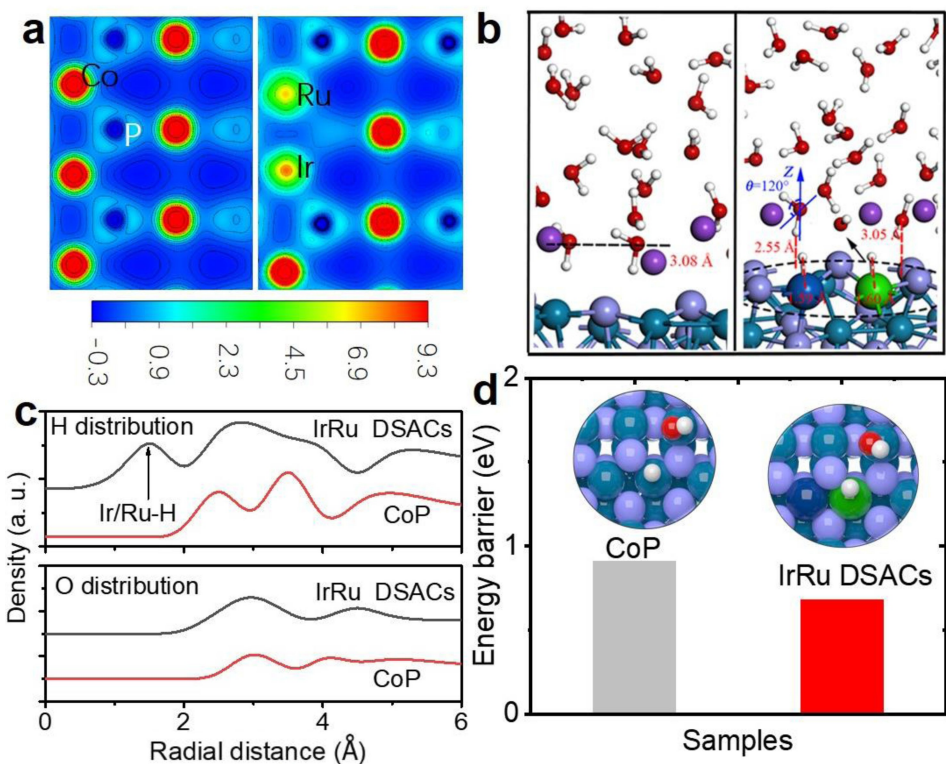


**Figure 2.** a) Charge density analyses of CoP and IrRu DSACs. b) Interfacial H<sub>2</sub>O orientation simulated by ab initio molecular dynamics (AIMD) simulations, and the statistical H and O distribution distance (c) in the z-direction of the adsorbed H<sub>2</sub>O molecules at the interface. The energy barriers and structures of H<sub>2</sub>O dissociation process (d) on the CoP and IrRu DSACs, calculated by DFT calculation.

microscopy (TEM) images and energy dispersive x-ray spectroscopy (EDS) mapping show the IrRu DSACs are uniformly distributed on the CoP matrix (Figure S5), which could be further confirmed by the X-ray diffraction (XRD) signals of only CoP (Figure S6). The Ir, Ru and Co ratios quantified by the inductively coupled plasma - optical emission spectrometry (ICP-OES) show that the number of Ir and Ru is identical before and after HER reaction (Table S2). High-resolution scanning TEM (HR-STEM) images show that Ir and Ru atoms appear in pairs, as the red circles marked in Figure 3a. The calculated average distance of Ir–Ru pairs is ca.  $0.249 \pm 0.015$  nm (Figure 3b), which is consistent with the DFT models and confirms the structure of IrRu DSACs.

To further understand the local structure of IrRu DSACs, the extended X-ray absorption fine structure (EXAFS) investigations were performed (Figure 3c and d).<sup>[9]</sup> The Ir L-edge spectra show that the IrRu DSACs possess Ir–P and Ir–Ru peaks at  $\approx 1.80$  and  $\approx 2.31$  Å, respectively (Figure 3c). The Ir–P peak at  $\approx 1.80$  Å in IrRu DSACs aligns well with that in Ir SACs and the strong Ir–Ru peak indicates Ir bonded with the adjacent Ru atoms. Similar, the peaks near to  $\approx 1.50$  and  $\approx 2.31$  Å belong to Ru–P and Ru–Ir bonds, respectively (Figure 3d). Combing the STEM and EXAFS results, we can conclude the formation of IrRu DSACs, consistent with the theoretical model (Figure S1).

To investigate the local electrical field of IrRu DSACs, the integral differential phase contrast-STEM (iDPC-STEM) was carried out (Figure 3e, f and S7). The thickness of the nanosheets are  $\approx 1$  nm, which - together with the low power of the incident electron beam—enables accurate charge density mapping. Notably, the IrRu DSACs possess a high average charge density variation of  $\approx 4.00$  e Å<sup>-2</sup> even under the linear charge density analysis, corresponding to an electric field intensity of  $\approx 4 \times 10^{10}$  N/C (Figure 3f, g and S8). In comparison, the Ir and Ru SACs possess only  $\approx 2.24$  and  $\approx 2.12$  e Å<sup>-2</sup> (Figure S8), respectively, which are much lower than that of IrRu DSACs. These results demonstrate that an obvious charge redistribution occurs on IrRu DSACs, which leads to enhanced atomic electric fields around IrRu active sites.

In order to reveal the interfacial H<sub>2</sub>O structure, in situ Raman tests were carried out (Figure 4). The stretching vibration peak of H<sub>2</sub>O on IrRu DSACs shifts from 1609 to 1618 cm<sup>-1</sup>, indicating the asymmetric H<sub>2</sub>O adsorption with H-down structure is formed on IrRu DSACs.<sup>[10]</sup> The envelope peaks at 3000–3600 cm<sup>-1</sup> can be deconvoluted into four peaks of 3000, 3200, 3388, and 3535 cm<sup>-1</sup>, corresponding to (HOH)<sub>n</sub>H<sup>+</sup> (hydrogen bonded water HBWn),<sup>[11]</sup> four hydrogen bonded water (4-HBW),<sup>[4a]</sup> two hydrogen bonded water (2-HBW),<sup>[4a]</sup> and K<sup>+</sup>·H<sub>2</sub>O (KW),<sup>[12]</sup> respectively. The HBWn and KW possess H-down structure. The proportions of various water structures are stable on IrRu DSACs at over  $-0.3$  V vs. RHE (Figure S9), indicating that the charge

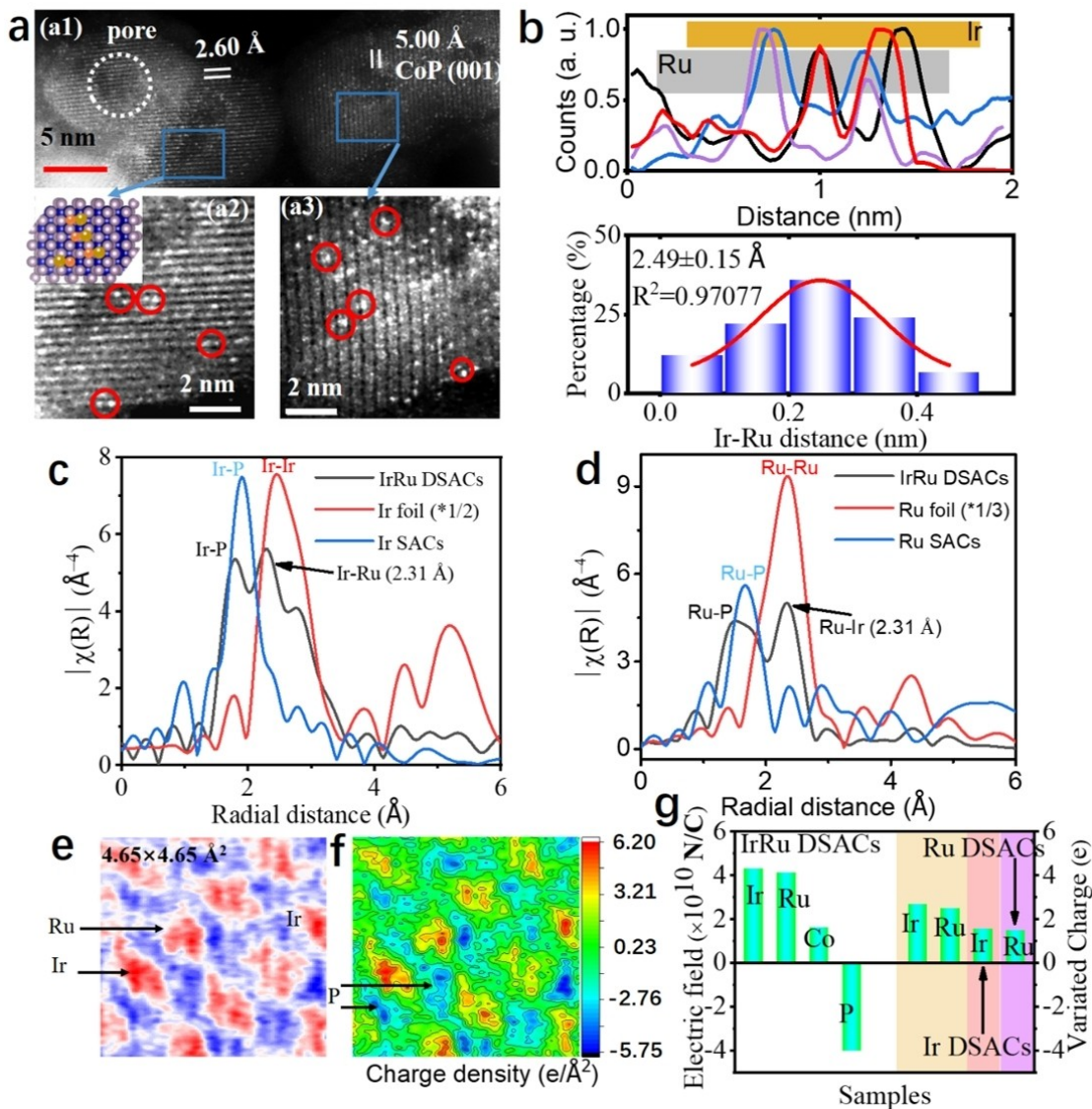


**Figure 3.** a) STEM image of IrRu DSACs. a1) is the low-resolution STEM image of IrRu DSACs. The rectangle marks the amplified area of IrRu DSACs with different exposed facet. a2) is the amplified area of CoP with lattice distance of 0.26 nm. Inset is the atomic model of IrRu DSACs. a3) is the amplified area of CoP with lattice distance of 0.5 nm. b) Atomic distribution of Ir–Ru pairs in IrRu DSACs. The top is the collection of the distance between Ir and Ru atoms. The bottom is the statistics of the distance of Ir and Ru atoms. c) Ir L-edge of Ir SACs, Ir foil and IrRu DSACs. d) Ru K-edge of Ru SACs, Ru foil and IrRu DSACs. The selected area integral differential phase contrast-STEM (e), corresponding quantified charge density (f). Total electric field and charge variations of Ir–Ru pairs in IrRu DSACs (g).

redistribution in IrRu DSACs possesses priority in modulating the water orientation over the applied potentials. The increased peak intensity of HBWn on IrRu DSACs demonstrates pseudo acidic environment at catalyst-electrolyte interface (Figure 4b). The HBWn and KW on IrRu DSACs have similar slopes of  $-12.14$  and  $-9.76$ , which are much smaller than those of 2-HBW (25.15), and 4-HBW (79.96) (Figure 4c), indicating that HBWn and KW with H-down structure are preferentially consumed during HER.

Comparatively, the in situ Raman peaks at  $1600 \text{ cm}^{-1}$  of CoP did not show obvious shifts (Figure 4d), indicating that the H-down structure is not easier formed on CoP. No HBWn signal is detected on the CoP (Figure 4d and e), revealing the poor water dissociation on CoP. The slopes of

2-HBW (8.44), 4-HBW (22.10) and KW (23.98) show that 2-HBW is preferentially consumed during HER (Figure 4f). These results confirmed that atomic electric fields on IrRu DSACs can induce  $\text{H}_2\text{O}$  adsorption configurations which promote its dissociation.

The alkaline HER of Ir–Ru DSACs was conducted in 1 M KOH. Compared to the polarization curves of IrRu DSACs, CoP NSs, Ru/C, and Pt/C (Figure 5a), the IrRu DSACs show the highest HER activity among those samples, even better than Ir, Ru SACs and IrRu alloy (Figure S10–S13). Besides, the IrRu DSACs possess ultra-high mass activity of  $2.36 \text{ mA ug}^{-1}$  at overpotential of 100 mV, higher than  $0.03 \text{ mA ug}^{-1}$  of CoP and  $0.63 \text{ mA ug}^{-1}$  of Ru/C, but low than  $4.81 \text{ mA ug}^{-1}$  of Pt/C. The lower Tafel

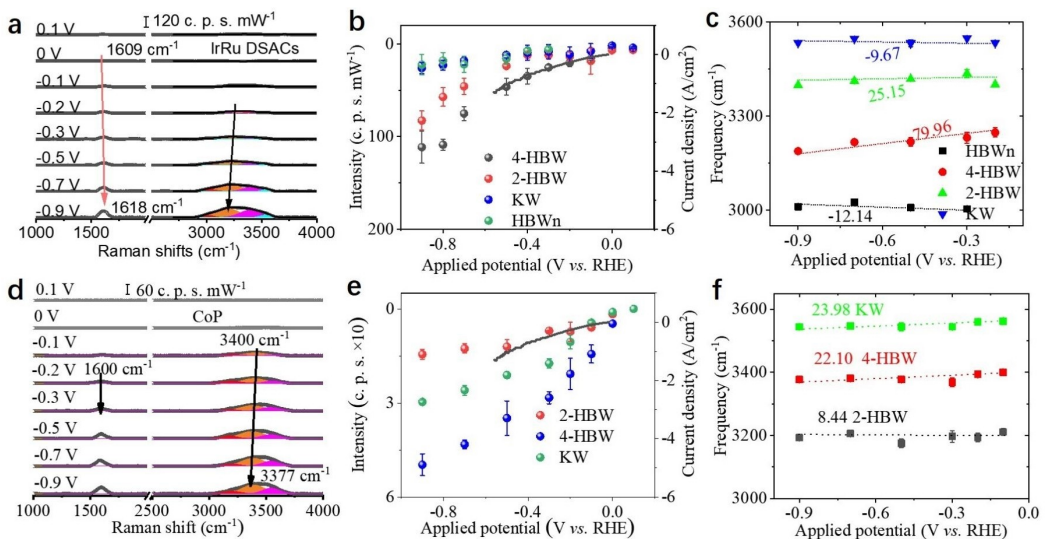


**Figure 4.** The in situ Raman spectra of IrRu DSACs (a) and corresponding specific peak intensity of various peak conducted form Raman spectra (b) and interfacial water structure evolution (c). The in situ Raman spectra of CoP (d) and corresponding specific peak intensity of various peak conducted form Raman spectra (e) and interfacial water structure evolution (f).

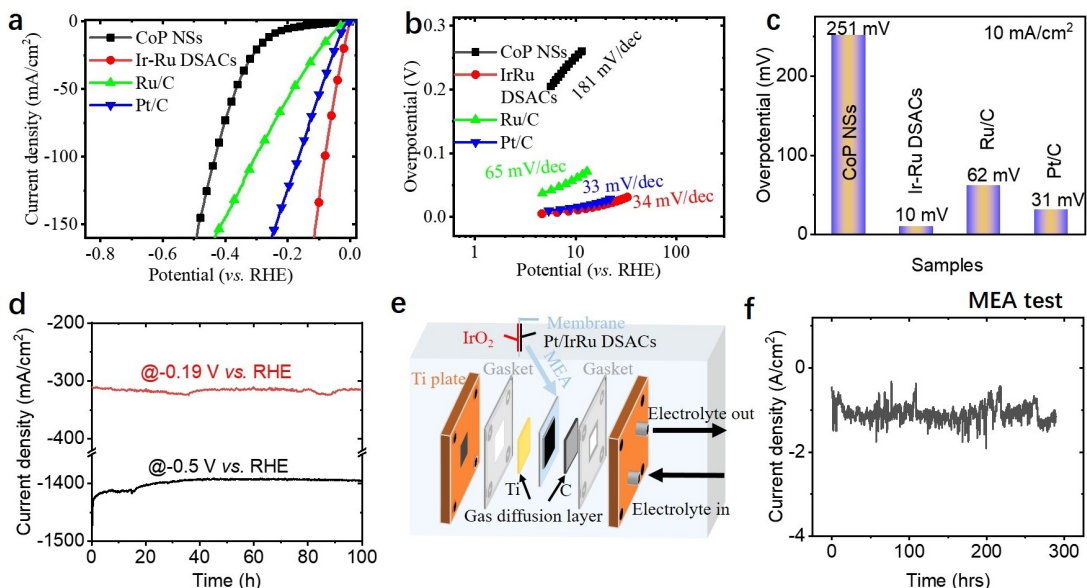


**Figure 5.** Electrochemical polarization curves (a), Tafel plots (b), and overpotentials at 10 mA cm<sup>-2</sup> (c) of the as-prepared catalysts (d) The accelerated degradation curve at a large current density of 1.4 and 0.3 A cm<sup>-2</sup> of Ir–Ru DSACs. e) MEA model test employed for DSACs. f) The stability test of IrRu DSACs in MEA at 1 A cm<sup>-2</sup>.

slope of Ir–Ru DSACs (22 mV dec<sup>-1</sup>), compared to those of CoP NSs (181 mV dec<sup>-1</sup>), Ru/C (65 mV dec<sup>-1</sup>), and Pt/C (33 mV dec<sup>-1</sup>), respectively, demonstrates the lower HER kinetic energy barrier for IrRu DSACs (Figure 5b). Thus, the IrRu DSACs exhibit an overpotential of only 10 mA cm<sup>-2</sup> at current density of 10 mA cm<sup>-2</sup>, which is lower than that of CoP NSs (251 mV), Ru/C(62 mV), and Pt/C (31 mV) and most reported values to date (Figure 5c and Table S3).<sup>[2c,13]</sup> Moreover, the IrRu DSACs show ultrahigh stability over 100 h at 300 mA cm<sup>-2</sup> and 1.4 A cm<sup>-2</sup> in single cells (Figure 5d). No obvious structure change and dissolution after long-time HER were observed by TEM and ICP measurements (Figure S14, S15 and Table S2).

To evaluate the practical applications of IrRu DSACs, the membrane electrode assembly (MEA) test was conducted (Figure 5e and f). The results show that IrRu DSACs only require low overpotentials of 78, 134, 286, and 500 mV to reach 0.1, 0.2, 0.5, and 1 A cm<sup>-2</sup>, respectively (Figure S16). Importantly, IrRu DSACs possess a high stability at 1 A cm<sup>-2</sup> in the MEA for over 300 h under an applied potential of –0.5 V, which is better than most reported values (Table S3).<sup>[13]</sup> These results demonstrate that the

IrRu DSACs can be a promising catalyst for the practical alkaline HER.

The concept that enhanced local electric fields can impact on molecular orientation and thus changing the chemical reaction rates can be extended to other molecules and catalysts, besides HER on IrRu DSACs. For instance, in photocatalysis, plasmonic structures can create highly-enhanced local electric fields, even at the atomic scale.<sup>[14]</sup> Of course, this light-induced fields are oscillating at high frequencies compared to the ones shown in here, but it could be worth exploring if a similar phenomenon to the one reported here can be also achieved with light or for other materials and molecules.

## Conclusion

In this work, IrRu DSACs were originally designed to generate an atomically asymmetric local electric field for tuning the H<sub>2</sub>O adsorption configuration and orientation, and thus promoting the alkaline HER. Our results indicate that the obtained IrRu DSACs exhibit an ultralow overpotential of 10 mV at 10 mA cm<sup>-2</sup> for alkaline HER and an ultrahigh stability in MEA at 1 A cm<sup>-2</sup> over 300 h, which are much better even than those of Pt/C and most reported catalysts. The quantitative results show that the IrRu DSACs possess charge density value of 4.00 e Å<sup>-2</sup>, which results in a strong atomically localized electric field, a reorientation of interfacial H<sub>2</sub>O and then the promoted H<sub>2</sub>O dissociation for better HER. These are confirmed by the AIMD simulations and Raman spectroscopy analyses which show the “H-down” adsorption configurations and reorientations of interfacial H<sub>2</sub>O by local electric fields. Our findings demonstrate that water orientation induced by atomically localized electric field can be an efficient way to achieve high HER activity.

## Additional Information

Supporting Information is available online for this paper.

## Acknowledgements

We thank the Natural Science Foundation of China (Grant No. 21872174, 52202125, 22002189, 22203105, 11874429, 12174450 and U1932148), Distinguished Youth Foundation of Hunan Province (2020JJ2041 and 2020JJ2039), Hunan Provincial Key Research and Development Program (2022WK2002), Project of High-Level Talents Accumulation of Hunan Province (2018RS3021), Hunan Provincial Natural Science Foundation of China (2020JJ5691). We are also grateful to Deutsche Forschungsgemeinschaft (DFG, German Research Foundation) under e-conversion Germany’s Excellence Strategy—EXC 2089/1—390776260, the Bavarian program Solar Energies Go Hybrid (SolTech), the Center for NanoScience (CeNS) and the European Commission through the ERC Starting Grant CATALIGHT

(802989). A.S. thanks the Alexander von Humboldt foundation for a postdoctoral fellowship. The XAS measurements were done at beamline 20-BM of the Advanced Photon Source, which is a Science User Facility of the U.S. Department of Energy (DOE) Office, operated by Argonne National Laboratory under Contract No. DE-AC02-06CH11357. We are grateful for the resources from the High Performance Computing Center of Central South University. Open Access funding enabled and organized by Projekt DEAL.

## Conflict of Interest

The authors declare no competing financial interest.

## Data Availability Statement

The data that support the findings of this study are available from the corresponding author upon reasonable request.

**Keywords:** Alkaline HER · Atomic Charge Distribution · Interfacial Water Orientation · Single-Atom Site · Water Dissociation

- [1] a) C. Cai, K. Liu, Y. Zhu, P. Li, Q. Wang, B. Liu, S. Chen, H. Li, L. Zhu, H. Li, J. Fu, Y. Chen, E. Pensa, J. Hu, Y. R. Lu, T. S. Chan, E. Cortes, M. Liu, *Angew. Chem. Int. Ed.* **2022**, *61*, e202113664; b) T. Chao, X. Luo, W. Chen, B. Jiang, J. Ge, Y. Lin, G. Wu, X. Wang, Y. Hu, Z. Zhuang, Y. Wu, X. Hong, Y. Li, *Angew. Chem. Int. Ed.* **2017**, *56*, 16047–16051; c) J. D. Yi, X. Gao, H. Zhou, W. Chen, Y. Wu, *Angew. Chem. Int. Ed.* **2022**, *61*, e202212329; d) X. Zhao, G. Wu, X. Zheng, P. Jiang, J.-d. Yi, H. Zhou, X. Gao, Z.-Q. Yu, Y. Wu, *Angew. Chem. Int. Ed.* **2023**, *62*, e202300879; e) W. Guo, X. Gao, M. Zhu, C. Xu, X. Zhu, X. Zhao, R. Sun, Z. Xue, J. Song, L. Tian, J. Xu, W. Chen, Y. Lin, Y. Li, H. Zhou, Y. Wu, *Energy Environ. Sci.* **2023**, *16*, 148–156; f) J. Wang, W. Liu, G. Luo, Z. Li, C. Zhao, H. Zhang, M. Zhu, Q. Xu, X. Wang, C. Zhao, Y. Qu, Z. Yang, T. Yao, Y. Li, Y. Lin, Y. Wu, Y. Li, *Energy Environ. Sci.* **2018**, *11*, 3375–3379; g) Y. Yao, S. Hu, W. Chen, Z.-Q. Huang, W. Wei, T. Yao, R. Liu, K. Zang, X. Wang, G. Wu, W. Yuan, T. Yuan, B. Zhu, W. Liu, Z. Li, D. He, Z. Xue, Y. Wang, X. Zheng, J. Dong, C.-R. Chang, Y. Chen, X. Hong, J. Luo, S. Wei, W.-X. Li, P. Strasser, Y. Wu, Y. Li, *Nat. Catal.* **2019**, *2*, 304–313.
- [2] a) M. Cao, K. Liu, Y. Song, C. Ma, Y. Lin, H. Li, K. Chen, J. Fu, H. Li, J. Luo, Y. Zhang, X. Zheng, J. Hu, M. Liu, *J. Energy Chem.* **2022**, *72*, 125–132; b) G. Chen, H. Li, Y. Zhou, C. Cai, K. Liu, J. Hu, H. Li, J. Fu, M. Liu, *Nanoscale* **2021**, *13*, 13604–13609; c) K. Su, H. Liu, Z. Gao, P. Fornasiero, F. Wang, *Adv. Sci.* **2021**, *8*, 2003156; d) B. Liu, Y.-F. Zhao, H.-Q. Peng, Z.-Y. Zhang, C.-K. Sit, M.-F. Yuen, T.-R. Zhang, C.-S. Lee, W.-J. Zhang, *Adv. Mater.* **2017**, *29*, 1606521.
- [3] a) C.-Y. Li, J.-B. Le, Y.-H. Wang, S. Chen, Z.-L. Yang, J.-F. Li, J. Cheng, Z.-Q. Tian, *Nat. Mater.* **2019**, *18*, 697–701; b) D. Liu, X. Li, S. Chen, H. Yan, C. Wang, C. Wu, Y. A. Haleem, S. Duan, J. Lu, B. Ge, P. M. Ajayan, Y. Luo, J. Jiang, L. Song, *Nat. Energy* **2019**, *4*, 512–518; c) A. Montenegro, C. Dutta, M. Mammetkuliev, H. Shi, B. Hou, D. Bhattacharyya, B. Zhao, S. B. Cronin, A. V. Benderskii, *Nature* **2021**, *594*, 62–65; d) K.

- Zhang, X. Liang, L. Wang, K. Sun, Y. Wang, Z. Xie, Q. Wu, X. Bai, M. S. Hamdy, H. Chen, X. Zou, *Nano Res. Energy* **2022**, *1*, e9120032.
- [4] a) Y.-H. Wang, S. Zheng, W.-M. Yang, R.-Y. Zhou, Q.-F. He, P. Radjenovic, J.-C. Dong, S. Li, J. Zheng, Z.-L. Yang, G. Attard, F. Pan, Z.-Q. Tian, J.-F. Li, *Nature* **2021**, *600*, 81–85; b) Q. Chen, K. Liu, Y. Zhou, X. Wang, K. Wu, H. Li, E. Pensa, J. Fu, M. Miyauchi, E. Cortes, M. Liu, *Nano Lett.* **2022**, *22*, 6276–6284; c) Y. Zhou, Y. Liang, J. Fu, K. Liu, Q. Chen, X. Wang, H. Li, L. Zhu, J. Hu, H. Pan, M. Miyauchi, L. Jiang, E. Cortes, M. Liu, *Nano Lett.* **2022**, *22*, 1963–1970.
- [5] a) J. Chen, G. Liu, Y.-Z. Zhu, M. Su, P. Yin, X.-J. Wu, Q. Lu, C. Tan, M. Zhao, Z. Liu, W. Yang, H. Li, G.-H. Nam, L. Zhang, Z. Chen, X. Huang, P. M. Radjenovic, W. Huang, Z.-Q. Tian, J.-F. Li, H. Zhang, *J. Am. Chem. Soc.* **2020**, *142*, 7161–7167; b) X. Cui, H.-Y. Su, R. Chen, L. Yu, J. Dong, C. Ma, S. Wang, J. Li, F. Yang, J. Xiao, M. Zhang, D. Ma, D. Deng, D. H. Zhang, Z. Tian, X. Bao, *Nat. Commun.* **2019**, *10*, 86.
- [6] a) X. Wang, Y. Zheng, W. Sheng, Z. J. Xu, M. Jaroniec, S.-Z. Qiao, *Mater. Today* **2020**, *36*, 125–138; b) Y. Yang, Y. Qian, H. Li, Z. Zhang, Y. Mu, D. Do, B. Zhou, J. Dong, W. Yan, Y. Qin, L. Fang, R. Feng, J. Zhou, P. Zhang, J. Dong, G. Yu, Y. Liu, X. Zhang, X. Fan, *Sci. Adv.* **2019**, *6*, eaba6586.
- [7] X. Zhao, F. Wang, X.-P. Kong, R. Fang, Y. Li, *J. Am. Chem. Soc.* **2021**, *143*, 16068–16077.
- [8] C. Cai, B. Liu, K. Liu, P. Li, J. Fu, Y. Wang, W. Li, C. Tian, Y. Kang, A. Stefanču, H. Li, C.-W. Kao, T.-S. Chan, Z. Lin, L. Chai, E. Cortes, M. Liu, *Angew. Chem. Int. Ed.* **2022**, *61*, e202212640.
- [9] a) M. Wang, Z. Feng, *Chem. Commun.* **2021**, *57*, 10453–10468; b) M. Wang, Z. Feng, *Curr. Opin. Electrochem.* **2021**, *30*, 100803; c) M. Wang, L. Árnadóttir, Z. J. Xu, Z. Feng, *Nano-Micro Lett.* **2019**, *11*, 47.
- [10] M. Sovago, R. K. Campen, G. W. H. Wurpel, M. Müller, H. J. Bakker, M. Bonn, *Phys. Rev. Lett.* **2008**, *100*, 173901.
- [11] V. Buch, B. Sigurd, J. Paul Devlin, U. Buck, J. K. Kazimirski, *Int. Rev. Phys. Chem.* **2004**, *23*, 375–433.
- [12] S. R. Lowry, K. A. Mauritz, *J. Am. Chem. Soc.* **1980**, *102*, 4665–4667.
- [13] a) B. Zhang, G. Zhao, B. Zhang, L. Xia, Y. Jiang, T. Ma, M. Gao, W. Sun, H. Pan, *Adv. Mater.* **2021**, *33*, 2105400; b) L.-W. Chen, X. Guo, R.-Y. Shao, Q.-Q. Yan, L.-L. Zhang, Q.-X. Li, H.-W. Liang, *Nano Energy* **2021**, *81*, 105636; c) Y. Li, Y. Luo, Z. Zhang, Q. Yu, C. Li, Q. Zhang, Z. Zheng, H. Liu, B. Liu, S. Dou, *Carbon* **2021**, *183*, 362–367; d) Y. Qin, Z. Wang, W. Yu, Y. Sun, D. Wang, J. Lai, S. Guo, L. Wang, *Nano Lett.* **2021**, *21*, 5774–5781; e) H. Tan, B. Tang, Y. Lu, Q. Ji, L. Lv, H. Duan, N. Li, Y. Wang, S. Feng, Z. Li, C. Wang, F. Hu, Z. Sun, W. Yan, *Nat. Commun.* **2022**, *13*, 2024; f) W. Wu, J. Liu, N. Johannes, *Int. J. Hydrogen Energy* **2021**, *46*, 609–621; g) Y. Yang, P. Yang, L. Zhou, R. He, Y. Hao, J. Wang, R. Qiu, X. Zhao, L. Yang, *Appl. Surf. Sci.* **2021**, *565*, 150461; h) L. Yi, B. Feng, N. Chen, W. Li, J. Li, C. Fang, Y. Yao, W. Hu, *Chem. Eng. J.* **2021**, *415*, 129034; i) C. Zhang, X. Liang, R. Xu, C. Dai, B. Wu, G. Yu, B. Chen, X. Wang, N. Liu, *Adv. Funct. Mater.* **2021**, *31*, 2008298; j) Z. Zhao, W. Jin, L. Xu, C. Wang, Y. Zhang, Z. Wu, *J. Mater. Chem. A* **2021**, *9*, 12074–12079.
- [14] a) E. Cortés, L. V. Besteiro, A. Alabastri, A. Baldi, G. Tagliabue, A. Demetriadou, P. Narang, *ACS Nano* **2020**, *14*, 16202; b) S. Ezendam, M. Herran, L. Nan, C. Gruber, Y. Kang, F. Gröbmeyer, R. Lin, J. Gargiulo, A. Sousa-Castillo, E. Cortés, *ACS Energy Lett.* **2022**, *7*, 2, 778; c) A. Stefanču, L. Nan, L. Zhu, V. Chiş, I. Bald, M. Liu, N. Leopold, S. A. Maier, E. Cortés, *Adv. Opt. Mater.* **2022**, *10*, 2200397.

Manuscript received: January 17, 2023

Accepted manuscript online: March 8, 2023

Version of record online: March 30, 2023